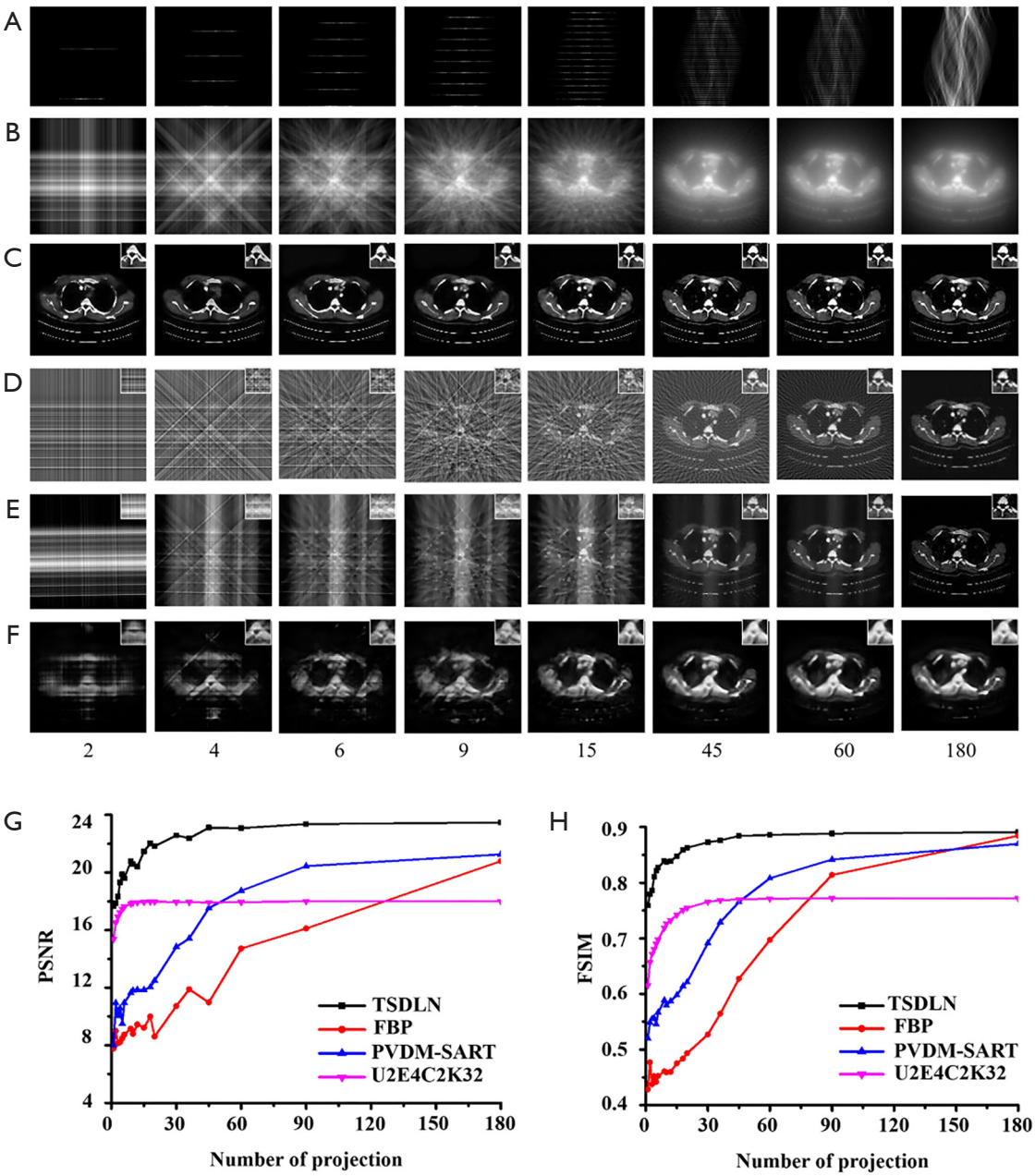

Figure S1 Accuracy verification of the proposed TSDLN-based reconstruction framework. (A,B) Sinograms and input BP images corresponding to 2, 4, 6, 9, 15, 45, 60, and 180 projections. (C-F) Reconstructed results by the TSDLN, FBP, PVDM-SART, and U2E4C2K32 respectively. The upper right corner of (C-F) is a partially-enlarged view of the reconstructed image. (G,H) PSNR and FSIM values as a function of projection number.

https://dx.doi.org/10.21037/qims-21-778

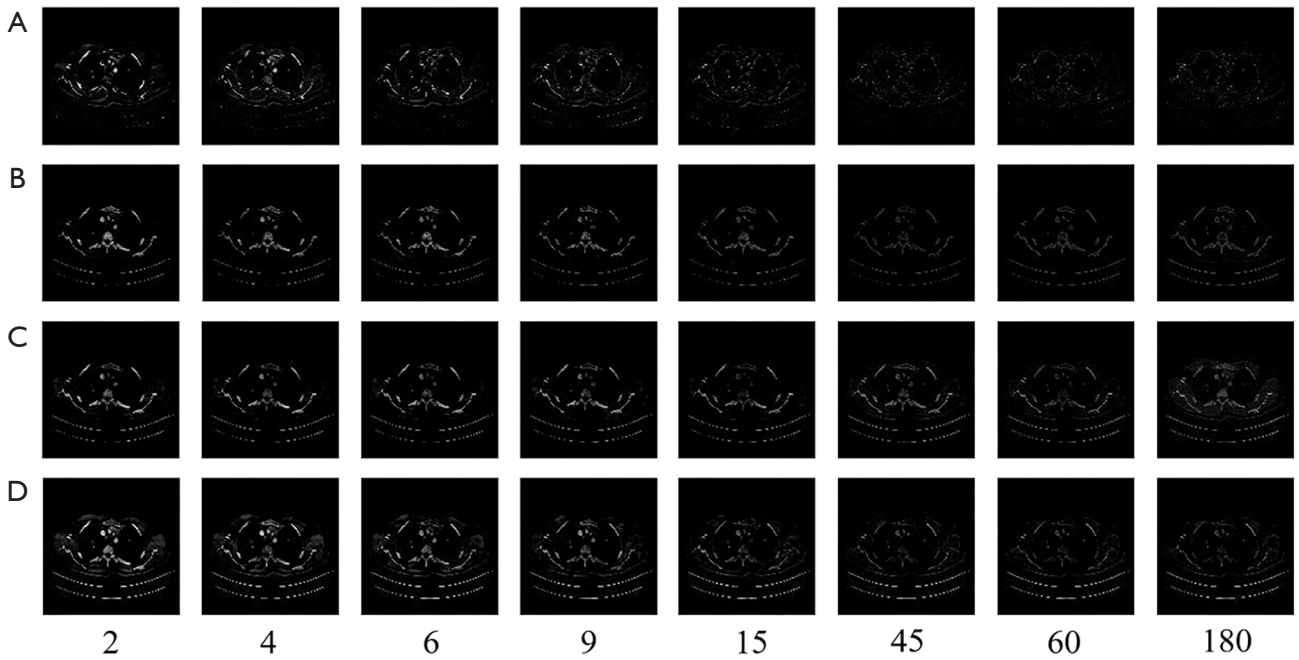

Figure S2 Difference images between the original and reconstructed images under projection number of 2, 4, 6, 9, 15, 45, 60, and 180. (A-D) Results the TSDLN, FBP, PVDM-SART and U2E4C2K32, respectively.

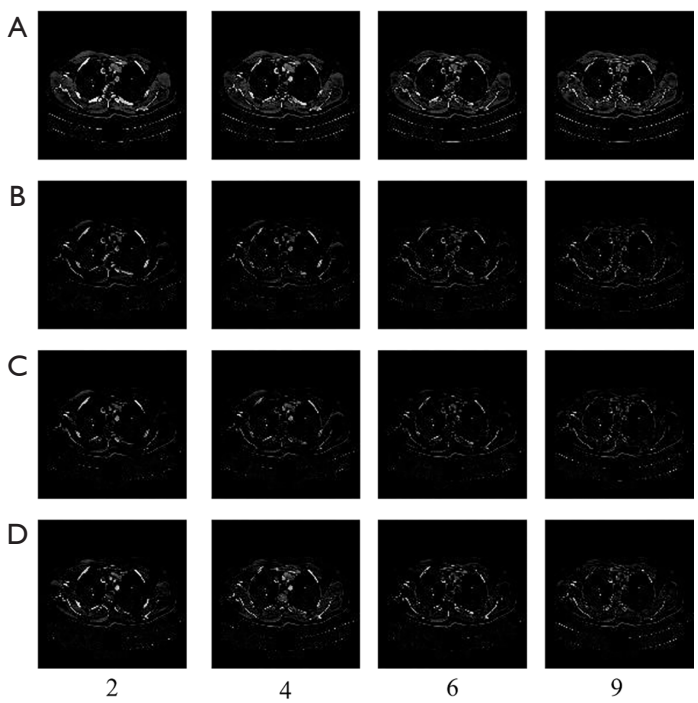

Figure S3 Difference images between the original and reconstructed images under projection number of 2, 4, 6, and 9. (A-D) Reconstructed results of Unet++, R_{l_U}, $R_{l_{U,SSIM}}$, and TSDLN, respectively.

https://dx.doi.org/10.21037/qims-21-778

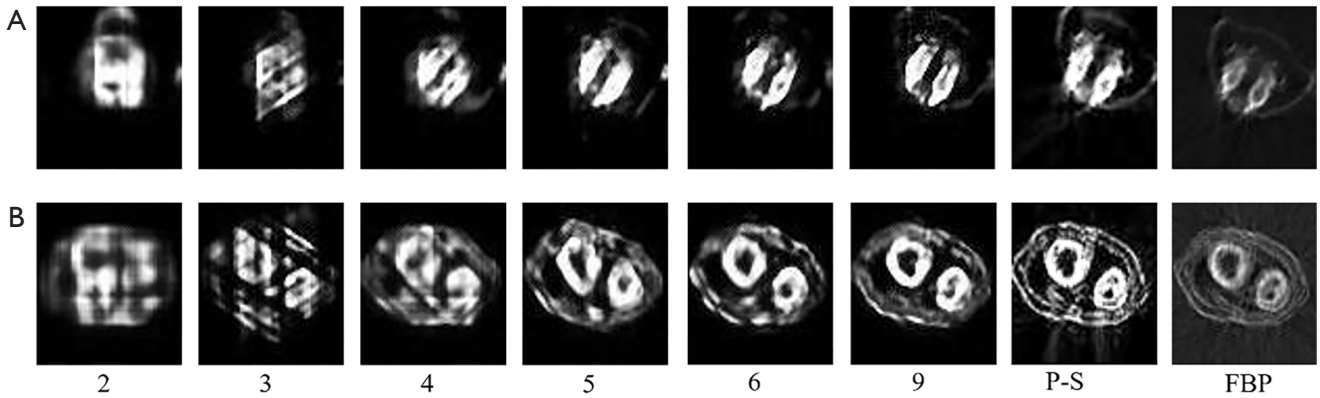

Figure S4 Verification results of migration capability of the proposed TSDLN based reconstruction framework. (A,B) Reconstructed results of the Drosophila and Arabidopsis silique respectively by using the TSDLN under 2, 3, 4, 5, 6, and 9 projections, as well as using the PVDM-SART(P-S) and FBP under 180 projections.

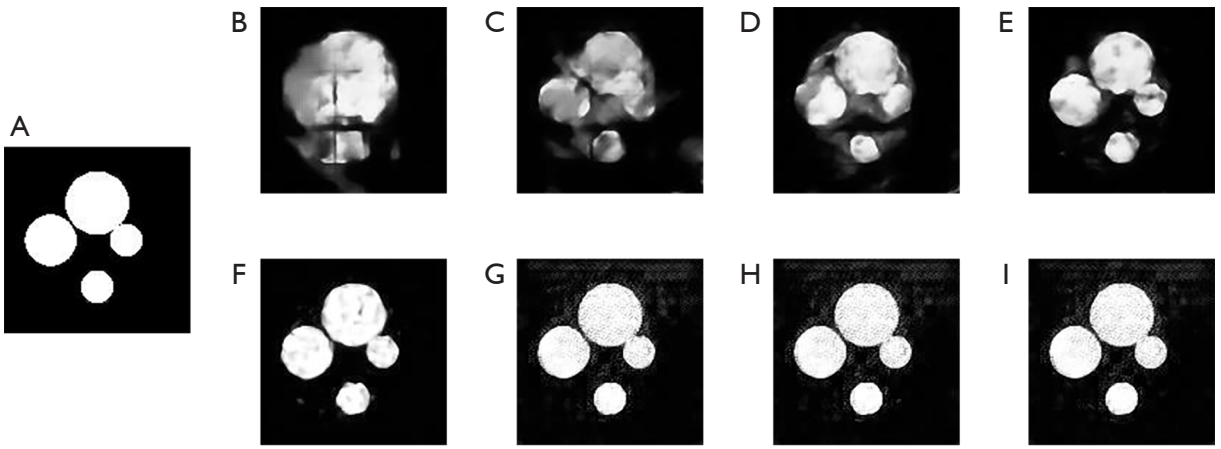

Figure S5 Reconstruction of digital phantom under different projections. (A) G-T image; (B-I) Reconstructed images of the TSDLN by using 2, 4, 6, 9, 15, 45, 60, and 180 projections, respectively.

https://dx.doi.org/10.21037/qims-21-778

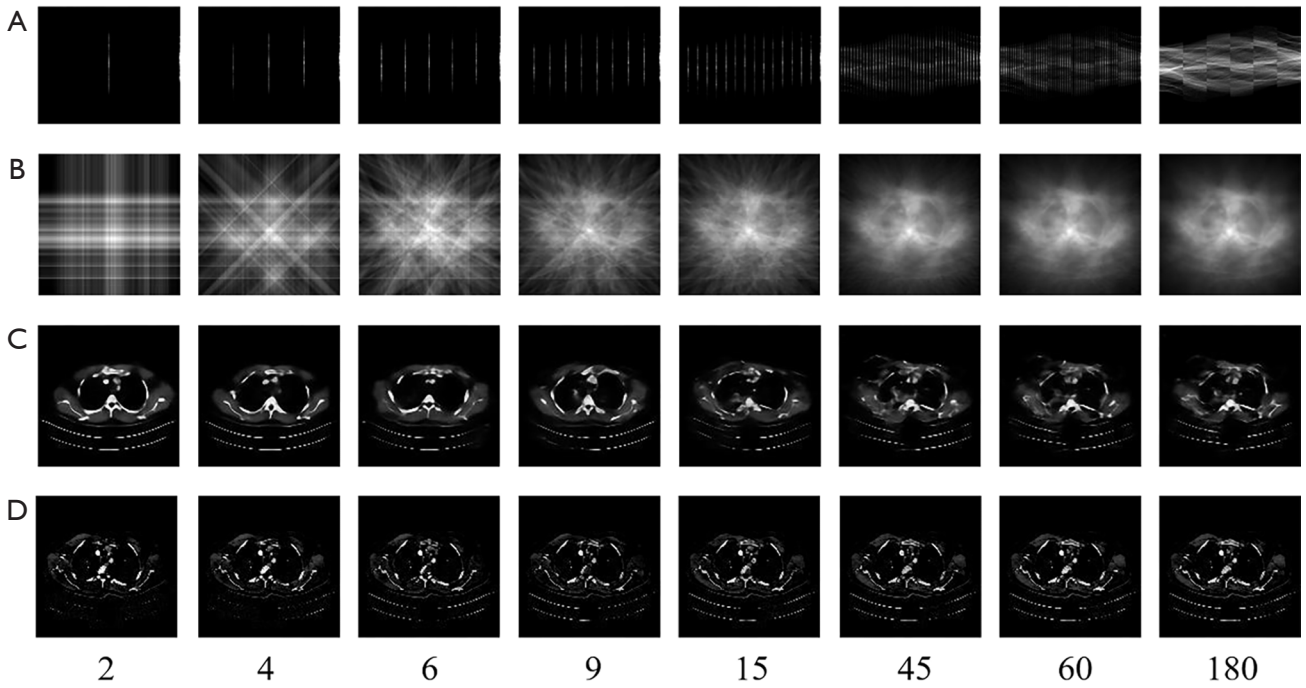

Figure S6 Reconstructed images with misalignment in the sinogram. (A,B) Sinograms and input BP images corresponding to 2, 4, 6, 9, 15, 45, 60, and 180 projections; (C) reconstructed images using 2, 4, 6, 9, 15, 45, 60, and 180 projections, respectively; (D) difference images between the original and reconstructed images under different projections.

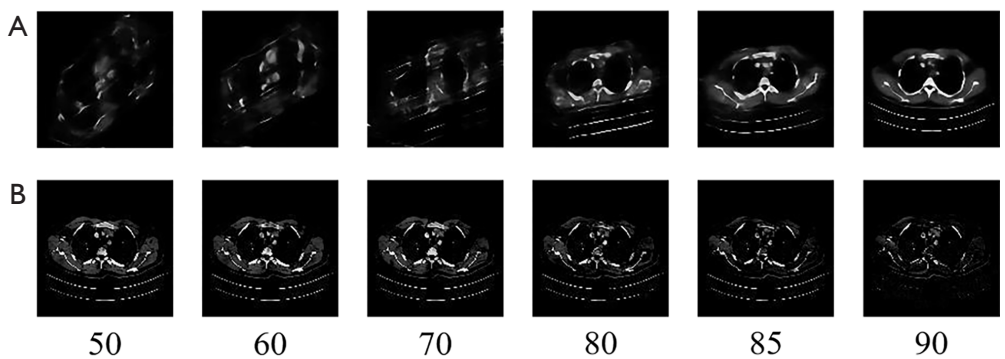

Figure S7 Reconstructed images using two projections from incorrect angles. (A) Reconstructed images by TSDLN using two projections from incorrect angles. One projection was fixed at the 90th angle, and the other projection was selected as the 180th, 175th, 170th, 160th, 150th, and 140th angle respectively; (B) Difference images corresponding to (A). Here, the 50, 60, 70, 80, 85, and 90 represent the angle interval between two projections used for reconstruction.

https://dx.doi.org/10.21037/qims-21-778

Table S1 Other evaluation factors for different reconstruction networks

		1	2	3	4	5	6	9
MSE	Unet++	1,607.377	1,311.215	1,178.01	1,080.646	1,018.039	955.8351	840.3254
	R_{lu}	1,663.745	1,309.601	1,121.755	998.8598	902.2595	820.391	659.3591
	R_{lSSIM}	1,720.699	1,301.623	1,101.031	969.5406	861.3696	785.5268	642.8228
	TSDLN	1,640.746	1,299.265	1,066.525	918.113	842.9279	761.0366	579.5668
RMSE	Unet++	39.5961	35.7471	33.9033	32.4684	31.5114	30.5243	28.59621
	R_{lu}	40.2048	35.6916	33.0335	31.1165	29.5642	28.1723	25.1863
	R_{lSSIM}	40.8849	35.5367	32.6751	30.6224	28.8441	27.5290	24.8392
	TSDLN	40.0160	35.5342	32.2031	29.8121	28.5488	27.1148	23.5979
NMSE	Unet++	0.6113	0.4985	0.4494	0.4126	0.3892	0.3661	0.3222
	R_{lu}	0.6449	0.5046	0.4309	0.3821	0.3449	0.3135	0.2517
	R_{lSSIM}	0.6691	0.5003	0.4232	0.3721	0.3286	0.3001	0.2446
	TSDLN	0.6369	0.5005	0.4118	0.3509	0.3223	0.2925	0.2226

https://dx.doi.org/10.21037/qims-21-778